Search for an ac Josephson effect in superfluid ^{4}He using a low-frequency acoustic resonator

B. P. Beecken and W. Zimmermann, Jr.
Tate Laboratory of Physics, University of Minnesota, Minneapolis, Minnesota 55455
(Received 21 July 1986)

A search for a Josephson effect in superfluid ^{4}He has been carried out with use of a low-frequency acoustic resonator in analogy to an rf-biased superconducting quantum interference device. Orifices from 100 to 400 nm in diameter in free-standing foils ~ 100 nm thick were used as weak links. Observations were made at temperatures from 0.4 to 1.1 K and at pressures from 13 to 40 kPa. Aside from the suggestive behavior seen in one early run, no sign of a Josephson effect has been observed. Values of the order-parameter phase difference through the weak link at the critical rate of flow ranged from $9\times 2\pi$ to $33\times 2\pi$ rad at $T=0.95$ K.

I. INTRODUCTION

The Josephson effects are fundamental aspects of the behavior of superconductors,[1] and parallel effects have been proposed for superfluid ^{4}He.[2,3] When this work was begun, a number of searches had been made for such effects in superfluid ^{4}He,[2,4–15] but considerable doubt existed as to whether any such effects had been observed.[16] This article describes a search for an effect in ^{4}He by a new method which was expected to improve the likelihood of observing such an effect.[17,18] Aside from the suggestive behavior seen in one early run, the present search has been unsuccessful in finding evidence for Josephson-effect behavior. We note, however, that a positive result has been reported recently from a closely related experiment,[19] suggesting further directions for study.

A. Josephson-effect principles for superfluid ^{4}He

In superconductors, the Josephson effects involve the behavior of several different kinds of weak links between bulk superconductors. The first effect, the dc effect, is given in its purest form by the equation

$$I_s = I_{sc}\sin(\Delta\phi) , \tag{1}$$

where I_s is the superconducting current flow through the weak link, I_{sc} is its limiting value, and $\Delta\phi$ is the difference between the phases of the order parameters of the two superconductors. The second effect, the ac effect, is given by the equation

$$\hbar\frac{d\Delta\phi}{dt} = -2\Delta\mu , \tag{2}$$

where $\hbar$ is Planck's constant h divided by 2π and $\Delta\mu$ is the difference between the electrochemical potentials of the two superconductors, per electron.

In superconductors, these relations have usually been applied to weak links whose important dimensions are comparable to or less than the superconducting coherence length. In superfluid ^{4}He, the weak links that have been used in experiment so far, tiny pores and orifices, have all had dimensions large compared to the corresponding coherence length, which is of the order of interatomic distances except near T_λ. Under these circumstances, it should be possible to apply two-fluid hydrodynamics incorporating quantized circulation and vorticity for the superfluid component.[20] The question then is to what degree does this approach predict behavior in superfluid ^{4}He which is analogous to that described by Eqs. (1) and (2) in superconductors.

Consider the flow of the superfluid component from one reservoir of ^{4}He to another through a small passage between the two. Assume for simplicity that at each end of the passage the flow effectively converges from or diverges into a full hemisphere and that the flow is incompressible. Allow quantum vortices to be present in the superfluid. Following the ideas of Huggins,[21] we can regard the superfluid velocity field $\mathbf{v}_s(\mathbf{r})$ to be the superposition of a velocity $\mathbf{v}_{sp}(\mathbf{r})$ of simple potential flow and a velocity $\mathbf{v}_{sv}(\mathbf{r})$ due to the vortices. The velocity $\mathbf{v}_s$ can be expressed in terms of the phase $\phi(\mathbf{r})$ of the superfluid order parameter (in radians) by the equation

$$\mathbf{v}_s = \frac{\hbar}{m_4}\mathrm{grad}\phi , \tag{3}$$

where m_4 is the mass of the ^{4}He atom. Accordingly, ϕ can be expressed as the sum of $\phi_p(\mathbf{r})$, a single-valued function of position related to $\mathbf{v}_{sp}$, and $\phi_v(\mathbf{r})$, a multiple-valued function related to $\mathbf{v}_{sv}$ by equations of the same form as Eq. (3).

We define the phase difference $\delta\phi$ from a point in the first reservoir far from the passage (point 1) to a similar point in the second (point 2) by the integral

$$\delta\phi = \int_1^2 \mathrm{grad}\phi\cdot d\mathbf{r} = \frac{m_4}{\hbar}\int_1^2 \mathbf{v}_s\cdot d\mathbf{r} \tag{4}$$

along some path in the liquid. Similar expressions define $\delta\phi_p$ and $\delta\phi_v$ so that $\delta\phi=\delta\phi_p+\delta\phi_v$. By simple hydrodynamic arguments it can be shown that once the superfluid mass current I_s flowing through the passage from the first reservoir to the second is specified, $\mathbf{v}_{sp}(\mathbf{r})$ is determined everywhere, and $\delta\phi_p$ is determined uniquely, independent of the path of integration. The relationships

between I_s, $\mathbf{v}_{sp}(\mathbf{r})$, and $\delta\phi_p$ are linear, and in particular we can write

$$L_s I_s = \frac{\hbar}{m_4}\delta\phi_p \ , \tag{5}$$

where L_s is a constant which is analogous to electrical inductance. This hydrodynamic inductance can be expressed as $l_{\text{eff}}/(\rho_s S)$, where l_{eff} is an effective length of the passage, ρ_s is the superfluid density, and S is the minimal cross-sectional area of the passage.

When singly-quantized vortices are present, $\delta\phi_v$ will be in general nonzero and will depend upon the path of integration, with values differing from one another by integral multiples of 2π. The same will thus be true for $\delta\phi$. Another aspect of this situation may be seen by considering the way in which $\delta\phi_v$ for a fixed path of integration varies as a vortex crosses the path at some point. Before and after the crossing, changes in $\delta\phi_v$ will be continuous. At the crossing, however, $\delta\phi_v$ will jump by $\pm 2\pi$, as thus will $\delta\phi$.

In order to avoid such path dependence and path-dependent jumps we can introduce an explicitly multiple-valued phase difference

$$\Delta\phi = \delta\phi + 2\pi n, \quad n = 0, \pm 1, \pm 2, \ldots , \tag{6}$$

with the understanding that all values of n are present simultaneously and that the jump of $\pm 2\pi$ in $\delta\phi$ which occurs as a vortex crosses a particular path does not carry over into $\Delta\phi$. This multiple-valued $\Delta\phi$ is independent of path. We shall see below that the time variation of the order-parameter phase difference is more naturally described in terms of $\Delta\phi$ than in terms of $\delta\phi$. The quantity $\Delta\phi$ can be written as $\Delta\phi_p + \Delta\phi_v$, where $\Delta\phi_p$ equals $\delta\phi_p$ and $\Delta\phi_v$ is related to $\delta\phi_v$ by an equation of the same form as Eq. (6).

In the absence of vortices the relation between I_s and $\Delta\phi$ takes the form

$$L_s I_s = \frac{\hbar}{m_4}(\Delta\phi - 2\pi n), \quad n = 0, \pm 1, \pm 2, \ldots , \tag{7}$$

which is plotted as the straight lines in Fig. 1. It is interesting to note that for the case of an ideal Josephson junction obeying Eq. (1) in series with an ideal inductor, it is possible to obtain a multiple-valued relationship between I_s and $\Delta\phi$ which in some regards resembles Eq. (7).[22]

When, perhaps at some critical velocity, a single vortex is created which grows, moves, shrinks, and disappears so that its core crosses just once any path between points 1 and 2, we may imagine the system point to move from one line in Fig. 1 to an adjacent one as depicted in the figure by the curve, with its multiple images. For example, a vortex ring might be formed at the perimeter of the mouth of the passage and blown out into the second reservoir like a smoke ring, shrinking and vanishing in the interior of the fluid. Or, a segment of vortex line whose ends remain in contact with the walls might move across the opening of the passage. Because $\Delta\phi_v$ changes by $\pm 2\pi$ during such an event, we shall refer to this event as a

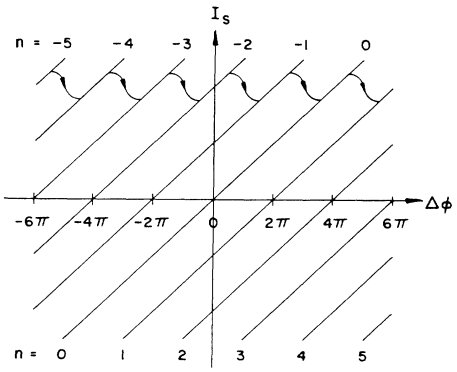

FIG. 1. Mass current I_s versus phase difference $\Delta\phi$. The straight diagonal lines show the various branches of $I_s(\Delta\phi)$ in the absence of vortices as given by Eq. (7). The curves show the multiple images of how I_s as a periodic function of $\Delta\phi$ might vary as a phase-slip event involving a single quantum vortex takes place.

phase-slip of $\pm 2\pi$, even though the change in $\Delta\phi$ which accompanies it may not be $\pm 2\pi$ if I_s changes at the same time, as is the case in the example shown in Fig. 1. Such an event is one for which a jump in $\delta\phi$ of $\pm 2\pi$ would have occurred at some instant for any path between points 1 and 2.

When more than one vortex is present, the situation is further complicated, and the number of possible states of the system corresponding to any one point in the I_s versus $\Delta\phi$ plane of Fig. 1 is further increased. Hence the situation for the dc effect may be summarized as follows. In place of the simple sinusoidal relation of Eq. (1) for superconductors, in which for each value of I_s between the limits $\pm I_{sc}$ there is a unique pair of values of $\Delta\phi \pmod{2\pi}$, the relation between I_s and $\Delta\phi$ for superfluid ^{4}He in the present limit is much more involved. For any given value of I_s there exists a continuum of values of $\Delta\phi \pmod{2\pi}$ arising from the wealth of possible vortex configurations and their corresponding values of $\Delta\phi_v$. The one element that is clearly common to both systems as we have formulated the problem is the periodicity in $\Delta\phi$.

We turn now to the ac effect. We assume that with vortices present we may write the superfluid equation of motion in the form[20,21]

$$\frac{\partial \mathbf{v}_s}{\partial t} - \mathbf{v}_s \times \text{curl}\mathbf{v}_s = -\text{grad}\left[\frac{\mu}{m_4} + \frac{v_s^2}{2}\right] + \mathbf{g} \ , \tag{8}$$

where μ is the chemical potential per ^{4}He atom. The quantity $\text{curl}\mathbf{v}_s$ is assumed to be zero everywhere but at the vortex cores, where it is effectively singular in such a way that

$$\int \text{curl}\mathbf{v}_s \cdot d\mathbf{S} = \pm\frac{h}{m_4} \tag{9}$$

for any surface spanning any contour surrounding a single core. The quantity $\mathbf{g}$ represents a local force per unit mass acting on the superfluid component at the vortex core arising from effects such as the motion of the core

relative to the normal-fluid component. This force is assumed to be zero everywhere but at the vortex core, where it is effectively singular in such a way as to yield a finite force per unit length of vortex core. Integrating Eq. (8) from point 1 to point 2 as defined in the discussion of the dc effect, we obtain

$$\frac{\hbar}{m_4}\frac{d\delta\phi}{dt}-\int_1^2(\mathbf{v}_s\times\mathrm{curl}\mathbf{v}_s+\mathbf{g})\cdot d\mathbf{r}=-\frac{\Delta\mu}{m_4}\ , \qquad (10)$$

assuming that $v_s^2/2$ is negligible at the end points.

As noted earlier, $\delta\phi$ will change continuously except for jumps of $\pm 2\pi$ as a vortex core crosses the path of integration. However, it can be shown that the integral in Eq. (10) expresses the rate at which vorticity is transported across the path. It follows with the aid of Eq. (9) that during the same interval of time in which $(\hbar/m_4)\delta\phi$ jumps by $\pm h/m_4$, as a vortex core crosses the path of integration, the time integral of the line integral in Eq. (10) jumps by $\mp h/m_4$. Hence the vortex-crossing jumps in $\delta\phi$ are cancelled by the integral, and Eq. (10) can be written

$$\hbar\frac{d\Delta\phi}{dt}=-\Delta\mu\ . \qquad (11)$$

This is the ac Josephson equation for superfluid ^{4}He and is of the same form as Eq. (2) for superconductors, aside from the factor of 2 in the latter for paired electrons.

Dissipative terms involving the second viscosity coefficients have been omitted from Eq. (8), but because they appear in gradient terms, they will not contribute to the integral, Eq. (10), since we may assume that the arguments of the gradients, like $v_s^2/2$, are negligible at the end points.[20]

Thus we see that under the small-coherence-length conditions considered, it is possible to develop relationships analogous to the Josephson effects in superconductors on the basis of two-fluid hydrodynamics and quantization of vorticity. While the ac effect takes the same form as in the superconducting case, the dc effect is rather different in form than in the simple superconducting case and reflects the existence of much more freedom in the system. In particular, the dc effect would not be expected to yield a two-slit interference pattern of the type that is observed with two superconducting Josephson junctions in parallel in the presence of a magnetic field.

The discussion above defines the Josephson effects for ^{4}He that have been sought up to now by others and which are the subject of the current search. Perhaps some day it will prove possible to work with superfluid-^{4}He weak links whose crucial dimensions are comparable to the relevant coherence length. In that case it may be possible to explore a more general form of Josephson effect, of which the present form is but a special case, and to observe a dc effect more like the one given by Eq. (1).

It is useful to consider the energy transferred to the vortex system in the course of a phase-slip event from the source of the chemical potential difference $\Delta\mu$ in the presence of flow and from the kinetic energy of the potential flow of the superfluid itself. At the same time the energy of the vortex system will tend to be dissipated by motion of the vortices relative to the normal-fluid component and perhaps by motion of the ends of the vortices relative to the walls, through the action of the local force $\mathbf{g}$ referred to earlier.

Under the assumptions that the flow of the superfluid is incompressible and that all of the vortex energy is kinetic, we can write the total kinetic energy of the fluid E as the sum of the energy of potential flow E_p and the energy of vortex motion E_v.[21] The rate at which energy is supplied to the fluid by the source of the chemical potential difference can be written as

$$-I_s\frac{\Delta\mu}{m_4}=I_s\frac{\hbar}{m_4}\frac{d\Delta\phi}{dt}\ , \qquad (12)$$

and the rate at which energy is released by the change in kinetic energy of potential flow can be written

$$-L_sI_s\frac{dI_s}{dt}=-I_s\frac{\hbar}{m_4}\frac{d\delta\phi_p}{dt}\ . \qquad (13)$$

The total rate of energy transfer from these sources to the vortex system is then given by the sum

$$I_s\frac{\hbar}{m_4}\left[\frac{d\Delta\phi}{dt}-\frac{d\delta\phi_p}{dt}\right]=I_s\frac{\hbar}{m_4}\frac{d\Delta\phi_v}{dt}\ . \qquad (14)$$

For a complete $\pm 2\pi$ phase-slip event, the total energy supplied will be given by the time integral of this quantity as $\Delta\phi_v$ changes by $\pm 2\pi$.

B. Josephson-effect experiments for superfluid ^{4}He

A general approach to observing a Josephson effect under the conditions considered above is to try to synchronize an external signal with, or otherwise to sense more directly, discrete transitions in which a single quantum vortex moves through the system and a phase slip of $\pm 2\pi$ occurs leaving the system in its initial state.

There have been a number of experiments in the past of the Richards-Anderson type,[2,4–6,8–12,14] which bear a close analogy to the Anderson-Dayem experiment in superconductivity.[23] In these, the influence of first-sound irradiation on the flow of superfluid through a small orifice was studied in analogy to the influence of rf radiation on the I-V characteristic of a superconducting Josephson junction. In at least some of these experiments, acoustic resonances, rather than a Josephson effect, were shown to be playing a dominant role.[10–12,16] In a related experiment, second-sound irradiation was employed.[15]

Another type of experiment involved a torsion oscillator carrying a toroidal channel containing superfluid ^{4}He interrupted by a small orifice. This arrangement bore a close analogy to a superconducting loop containing a single Josephson junction inductively coupled to an rf tank circuit as in an rf-biased superconducting quantum-interference device (SQUID).[7] An experiment looking for the interference between two weak links has also been performed.[13] Nevertheless, considerable doubt exists as to whether a Josephson effect has been observed in any of these experiments, and it was in this context that the experiment described in this article was undertaken.

The experiment presented here uses a low-frequency acoustic resonator involving a closed flow loop for the liquid. This loop contains a single tiny orifice, which con-

stitutes the weak link. This system is analogous to the rf-biased SQUID in several ways, and, because of this, is more closely related to the torsion-oscillator experiment than to the other Josephson-effect experiments on superfluid ^{4}He mentioned above.

In designing this experiment we sought to satisfy two criteria which were not well satisfied in at least some of the previous searches. As a result we were led not only to the low-frequency resonator design but also to use as our weak links orifices which were one or two orders of magnitude smaller in dimension than orifices that were used in previous experiments.

The first criterion concerns $\delta\phi_c$, the value of $\delta\phi=\delta\phi_p$ evaluated through the weak link orifice at (i.e., just below) the critical rate of flow, where vortex motion and phase slip first occur. It is highly desirable that $\delta\phi_c$ be no larger than several times 2π. To see why, note first that in order for the phase slip to be synchronized with some external signal, it is important that each time phase slip occurs it takes place in a reproducible manner. Suppose that the phase slip occurs on a time-scale short compared to that on which $\Delta\phi$ varies, as governed by Eq. (11). Then phase slip to a smaller value of $\delta\phi$ involves a vertical transition in Fig. 1. If $\delta\phi_c$ is small, the number of final states is very restricted, and this restriction should enhance reproducibility.[3]

Minimizing $\delta\phi_c$ involves minimizing the product of the effective hydrodynamic length of the orifice $l_{\rm eff}$ and the effective critical velocity in the orifice v_{sc}. The effective length of an orifice or pore is of order $l+d$, where l is the actual length of the pore (or the thickness of the wall containing the orifice) and d is the diameter of the orifice. Although we do not know how v_{sc} for an orifice or pore depends on l, past results from long-pore experiments suggest that v_{sc} increases with decreasing d, but less rapidly than d^{-1}. If we assume that v_{sc} is independent of l, we are led to the conclusion that we should decrease l and d as much as possible, maintaining $l\leq d$. It is interesting to note that for such a pore a Feynman-like critical velocity $v_c=[\hbar/(m_4 d)]\ln(d/a)$ with a of the order of interatomic distances yields $\delta\phi_c$ of order 2π.[24]

Most of the previous experiments of the Richards-Anderson type have employed orifices having diameters d ranging from 10 to 20 μm and lengths l from 15 to 50 μm. Critical velocities in these orifices have ranged from 10 to 400 mm/s. If we take representative values $d=15$ μm, $l=20$ μm, and $v_{sc}=200$ mm/s, then we have $\delta\phi_c=70\times 2\pi$. Under such conditions our first criterion would be strongly violated.

The second criterion concerns the time required for the system to recover after phase slip occurs. If phase-slip events are to be reproducible it is highly desirable that the vortex motion associated with any given event be complete before the next event occurs. This criterion also favors orifices with small diameters and lengths, so that vortices, in either moving across the opening or escaping from it, have shorter distances to cover. At the same time the higher critical velocities and self-induced vortex velocities associated with such orifices should also help to shorten the recovery time. Furthermore, the second criterion favors lower frequencies of operation with which the events are to be synchronized.

Using d/v_{sc} as a measure of the recovery time, we find a value of 75 μs under the representative conditions cited above. This value is long compared to the 10-μs period of oscillation for the widely-used frequency of 100 kHz in Richards-Anderson—type experiments. Hence for such conditions the second condition would be strongly violated.

Thus we were led to try using smaller orifices in thinner films and lower frequencies of operation than had been used in previous Richards-Anderson—type experiments. We note, however, that somewhat more favorable conditions than the representative conditions above existed in the torsion oscillator experiment of Guernsey.[7] In that experiment, an orifice as small as 0.8 μm in diameter in a foil 2.5 μm thick was tried at an oscillator frequency of 450 Hz. As a practical goal we chose to use single orifices as small as 100 nm in diameter in foils 100 nm thick for our weak links, and to use a low-frequency resonator method which permitted the use of frequencies of oscillation of the order of 1000 Hz and below. Nevertheless, aside from some suggestive results that we obtained in the early stages of this work,[17] we have been unable to see signs of Josephson behavior in our experiment. A preliminary report of the determination of $\delta\phi_c$ for a number of small orifices in the course of this work was given in Ref. 18.

Recently, other workers have reported success in directly observing discrete 2π phase-slip events at an orifice.[19] Their experiment incorporates some of the same features that we have considered important, using a low-frequency resonator and a micrometer-size orifice in a thin film. However, their technique is somewhat different from ours, and they have used very much lower frequencies and temperatures.

II. EXPERIMENTAL APPARATUS AND PRINCIPLES OF OPERATION

A. Apparatus

The cell used for this work, shown schematically in Fig. 2, consisted of two chambers which were completely filled with liquid ^{4}He. The chambers were separated by a partition with two openings which connected the chambers. One of these, the main passage, had a relatively large total open cross-sectional area, which in some runs was occupied or covered by a porous medium so as to form a superleak. The other opening, the weak link, was a tiny orifice in a thin free-standing nickel foil.

The upper wall of the upper chamber was a flexible diaphragm and was driven by a piezoelectric cylinder in order to excite fluid motion between the chambers. The lower wall of the lower chamber was also a flexible diaphragm and had fastened to it the movable plate of a variable capacitor. This arrangement was used to sense the motion of the fluid in response to excitation.

The cell, when filled with liquid, possessed two principal low-frequency resonances resulting from the coupling of two ideal resonances. One of these ideal resonances was a Helmholtz resonance involving oscillatory flow of

the fluid between the two chambers through the main passage and weak link in parallel, without diaphragm motion. The other ideal resonance involved oscillation of the lower diaphragm in the absence of fluid.

When the main passage was open, so that both normal-fluid and superfluid motion could take place freely, the Helmholtz resonance was a first-sound Helmholtz resonance. In fact, in this case a second-sound Helmholtz resonance, involving countermoving normal fluid and superfluid, would also have been present. However, such a resonance would not have coupled strongly to diaphragm motion and was not expected to be observed. When the main passage was a superleak, the Helmholtz resonance was a fourth-sound Helmholtz resonance with stationary normal-fluid component.

The upper diaphragm would also have been expected to have a resonance, but this diaphragm was stiffened by the piezoelectric transducer and carried less mass than the capacitor plate attached to the lower diaphragm. As a result its resonant frequency was considerably higher than that of the lower diaphragm and was not taken into account.

In the case of the open main passage, the interior of the cell formed a flow loop involving the main passage and the weak link. In the case of the superleak main passage, there were many such flow loops in parallel. Thus the cell was analogous to an rf-biased SQUID involving a superconducting loop interrupted by a single weak link. Either one of the two resonances in our cell played the role of the resonance of the rf tank circuit of the SQUID.

With reference to Fig. 2, the center piece of the cell which formed the wall between chambers was made of oxygen-free high-conductivity (OFHC) copper. Disks of copper or brass 6 mm in diameter and 0.5 mm thick bearing the weak link and main passage were pressed into recesses surrounding 3.2-mm-diam openings in this piece using 0.5-mm-diam indium wire as gasket material. Separate fill capillaries for the two chambers entered through this piece, two germanium resistance thermometers were embedded in grease in two external holes in this piece, and a ~ 500-Ω heater was fastened to the piece.

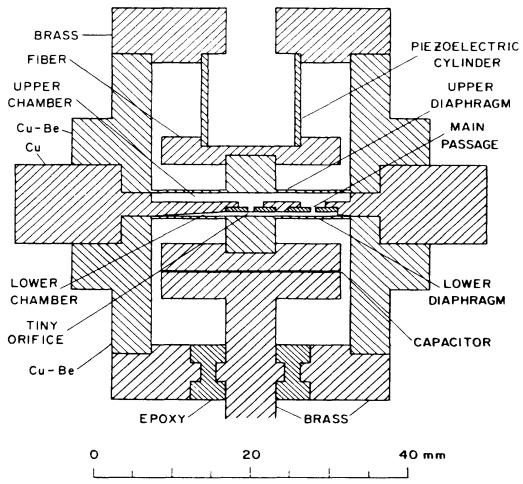

FIG. 2. Schematic scale drawing of the cell.

Each of the weak-link orifices used in this work has consisted of a single irregular but more or less circular opening from 100 to 400 nm in diameter in a 100 or, in one case, 200-nm-thick nickel film that was free-standing over a circular region ~ 30 μm in diameter. The nickel film was supported at the edge of this region by a 5-μm-thick copper foil to which it was bonded. The copper foil was glued with epoxy cement[25] over a 0.8-mm-diam hole in a disk of the type mentioned above that was mounted in the hole in the middle of the center piece. The fabrication of these weak-link orifices is described in Ref. 26.

For many of the runs, the main passages consisted of openings from 0.3 to 0.8 mm in diameter drilled in either the same disk carrying the weak-link orifice or in another disk offset from the axis of the cell by 7.9 mm, as shown in Fig. 2. In three runs the entire 3.2-mm-diam offset opening in the center piece of the cell served as main passage, and in one run the main passage consisted of a nearly circular opening 29 μm in diameter in a copper foil 5 μm thick. For the runs in which the main passages were superleaks, use was made of a 0.8-mm-diam hole either pressed full of 0.05-μm alumina powder[27] or covered at one end by a Nuclepore filter membrane with 30- or 80-nm-diam pores,[28] glued to the disk with epoxy cement.[25]

The upper and lower chambers were formed by two identical caps of heat-treated beryllium copper.[29] These caps had diaphragms approximately 0.35 mm thick formed by machining. The caps were demountable and were held to the center piece with screws and sealed to it using 0.5-mm-diam indium wire gaskets. The upper and lower chamber volumes were estimated from cell dimensions to be 0.71 and 0.17 cm^3, respectively. In several runs these chambers were filled to the extent possible with a porous filter material having 1.2-μm pores.[30]

The piezoelectric driver cylinder[31] was anchored to a brass cover plate screwed down to the top of the upper cap and was coupled to the driver diaphragm by means of a fiber disk. The capacitor plate attached to the lower diaphragm was 22.9 mm in diameter and had a mass of 13 g. A fixed plate below it formed the remainder of the capacitor. A representative value for the capacitance when the diaphragm was relaxed was ~ 125 pF, corresponding to a plate spacing of ~ 30 μm. This capacitor constituted most of the tank capacitance of a small back-diode rf oscillator which was mounted directly on the bottom of the cell. The oscillator used a General Electric BD-5 back diode, oscillated at ~ 9 MHz when the diaphragm was relaxed as above, and dissipated ~ 7 μW at the bias voltage normally used.

The cell was cooled by means of a conventional ^{3}He refrigerator employing pumped ^{3}He and ^{4}He pots and a ^{4}He bath at atmospheric pressure. Glass Dewars were used for the ^{4}He bath and the surrounding liquid-nitrogen bath. One unusual feature of the cryostat was that the cell was freely suspended on springs below the ^{3}He pot to reduce the influence of external vibration. The translational and torsional frequencies of the suspension were several hertz. For the same reason the cryostat as a whole was mounted

on a two-stage vibration isolation platform, with flexible pumping-line connections.

A second unusual feature was that in order to reach temperatures down to slightly below 0.4 K in our cryostat it was found most convenient to mount a second pumped ^{3}He pot directly on the cell support ring. This small pot, of approximately 1-cm^3 volume, rode with the cell on its suspension and was pumped in one-shot mode through flexible bellows below the main ^{3}He pot, which was run in continuous mode. The hold time of the small pot exceeded 12 h.

The cell was filled through capillaries which began at room-temperature valves at the top of the cryostat and ran down to the cell, with heat sinks to the main ^{4}He bath, the ^{4}He pot, and the upper ^{3}He pot. From the ^{4}He bath down, these capillaries had inner diameters of $\sim$0.2 mm, and the portions nearest the cell were filled with $\sim$60-mm lengths of 0.1-mm-diameter wire.

The piezoelectric driver cylinder was driven through a ratio transformer by a sinusoidal signal from a computer-controlled function generator synthesizer, which facilitated slow sweeps of frequency or amplitude near one of the resonances of the cell. The resulting frequency-modulated rf signal from the back-diode deflection-sensing oscillator was amplified and then mixed with an rf signal from a highly stable local oscillator to produce an intermediate-frequency signal of $\sim$50 kHz. This signal was fed to an fm discriminator whose output went to a two-phase lock-in amplifier which derived its reference signal from the function generator used to generate the drive signal. The resulting vector-sum output was recorded by computer and plotted using an X-Y recorder.

The average oscillator frequency, as read by a frequency counter, was used to monitor the average pressure in the cell. The deflection-sensing capacitor attached to the lower diaphragm thus functioned as both an ac and a dc pressure sensor between 0 and $\sim$50 kPa cell pressure.

The resistances of the two germanium thermometers were sensed using two separate ac bridges with lock-in detectors, either one of which could be used to drive an integrating regulator circuit connected to the cell heater in order to control cell temperature.

B. Principles of operation

1. Cell resonances

Here we develop a simplified model for the operation of the cell based on the two-fluid equations of motion for superfluid ^{4}He.[20] For the moment we consider only the main passage to be present, without the weak link. In the low-temperature limit, in which the liquid is assumed to be pure superfluid and any temperature variations are neglected, and in the absence of any vorticity in the superfluid, we find the following set of equations:

$$I=-\rho_1\frac{d\Omega_1}{dt}-\Omega_1\frac{d\rho_1}{dt}\cong\rho A\frac{dx}{dt}-\rho\kappa\Omega_1\frac{dP_1}{dt}\ , \tag{15}$$

$$I=\rho_2\frac{d\Omega_2}{dt}+\Omega_2\frac{d\rho_2}{dt}\cong\rho\frac{d\Omega_{2d}}{dt}+\rho\kappa\Omega_2\frac{dP_2}{dt}\ , \tag{16}$$

$$\frac{P_2-P_1}{\rho}=-L_m\frac{dI}{dt}\ , \tag{17}$$

$$-P_1A-kx=m\frac{d^2x}{dt^2}\ . \tag{18}$$

Here the subscripts 1 and 2 stand for the lower and upper chambers, respectively. The quantity I is the mass current from lower to upper chamber, Ω_i is the volume of the ith chamber, P_i is the pressure in the ith chamber, ρ_i is the fluid density in the ith chamber, κ is the compressibility of the fluid, A is the effective area of the lower diaphragm, x is the displacement of the center of that diaphragm from equilibrium in the upward direction, k is the effective spring constant of the diaphragm, m is the effective mass of the diaphragm together with the mass of the attached capacitor plate, $d\Omega_{2d}/dt$ is the rate of change of Ω_2 due to motion of the upper, drive diaphragm, and L_m is the hydrodynamic inductance of the main passage. The symbol L is used here for the main passage in the same sense that it was used in Sec. I A for the weak link. In these equations we have not included any dissipation. In addition, we have assumed that Ω_2 is not influenced by P_2 but depends only on the drive signal.

The first two equations express conservation of fluid mass in the lower and upper chambers, respectively. The third equation is the equation of motion for fluid flow through the main passage between chambers, and the fourth equation is the equation of motion of the lower diaphragm. By considering the work done by the fluid on the diaphragm it can be seen that the same effective area A which expresses the rate of change of Ω_1 with x in Eq. (15) expresses the relation between P_1 and force in Eq. (18).

We solve these simultaneous linear equations for steady-state sinusoidal motion, in which the physical solution is given by the real part of complex quantities proportional to $e^{i\omega t}$. Complex amplitudes will be designated by a subscript 0. Of most interest to us are the relationship between x_0 and Ω_{2d0} and the relationship between the amplitude of the chemical potential difference $\mu_{20}-\mu_{10}$ between chambers per atom and x_0. The solutions for these relationships are given by the expressions

$$x_0=\frac{A}{k\kappa(\Omega_1+\Omega_2)}\frac{\omega_T^2\omega_H^2}{(\omega^2-\omega_+^2)(\omega^2-\omega_-^2)}\Omega_{2d0}\ , \tag{19}$$

$$\mu_{20}-\mu_{10}=\frac{m_4}{\rho}\frac{k}{A}\frac{\Omega_1+\Omega_2}{\Omega_2}\frac{\omega^2}{\omega_H^2}\frac{(1+\alpha_1)\omega_T^2-\omega^2}{\omega_T^2}x_0\ . \tag{20}$$

Here we have

$$\omega_T^2=k/m\ , \tag{21}$$

$$\omega_H^2=\frac{1}{\rho^2\kappa L_m}\frac{\Omega_1+\Omega_2}{\Omega_1\Omega_2}=\frac{1}{\rho\kappa}\frac{S_m}{l_{\mathrm{eff},m}}\frac{\Omega_1+\Omega_2}{\Omega_1\Omega_2}\ , \tag{22}$$

and ω_+ and ω_- satisfy the equations

$$\omega_+^2+\omega_-^2=\omega_T^2(1+\alpha_1)+\omega_H^2\ , \tag{23}$$

$$\omega_+^2\omega_-^2=\omega_T^2(1+\alpha_t)\omega_H^2\ . \tag{24}$$

The dimensionless parameters α_1 and α_t are defined by

the expressions

$$\alpha_1 \equiv A^2/(k\kappa\Omega_1) , \tag{25}$$

$$\alpha_t \equiv A^2/[k\kappa(\Omega_1+\Omega_2)] . \tag{26}$$

The quantity ω_T is the resonant angular frequency of the lower diaphragm and capacitor plate in the absence of fluid, while ω_H is the Helmholtz resonant angular frequency that would occur for the case of an inflexible lower diaphragm; ω_+ and ω_- are the actual resonant angular frequencies which result from the coupling of these two ideal modes. When $\Omega_{2d0}=0$, the system is completely analogous to a linear chain of three springs separated from each other by two masses in which the masses are constrained to move only along the axis of the chain and the ends of the chain are fastened to fixed points.

When the derivation is not restricted to the low-temperature limit and full use of the two-fluid model is made, including temperature as well as pressure variations in the chambers, Eqs. (19) and (20) together with Eqs. (21) through (26) continue to be quite accurate over a wide range of experimental conditions with only minor modification. When an open main passage is used but the viscous penetration depth of the normal-fluid component remains small in comparison with the diameter of the passage, the principal change in these equations is the appearance of damping terms in the resonance denominator of Eq. (19) which limit the resonant response. In Eq. (22), for ω_H^2, L_m must be taken equal to $l_{\text{eff},m}/(\rho S_m)$. On the other hand, when a superleak main passage is used, so that the viscous penetration depth of the normal-fluid component is large in comparison to the diameters of the pores and the normal-fluid component is effectively prevented from flowing between chambers, L_m in the first part of Eq. (22) must be taken equal to $l_{\text{eff},m}/(\rho_s S_m)$, so that the second part must be replaced by[32]

$$\omega_H^2 \cong \frac{\rho_s}{\rho}\frac{1}{\rho\kappa}\frac{S_m}{l_{\text{eff},m}}\frac{\Omega_1+\Omega_2}{\Omega_1\Omega_2} . \tag{27}$$

Here, too, damping terms will be present in the denominator of Eq. (19).

2. *Detection of an ac Josephson effect*

Returning to the low-temperature limit, we now include the weak link in our model for the cell. Equations (15) and (16) remain valid with $I=I_w+I_m$, where I_w and I_m are the mass currents through the weak link and main passage, respectively. Equation (17) becomes

$$\frac{P_2-P_1}{\rho} = -L_w\frac{dI_w}{dt} = -L_m\frac{dI_m}{dt} , \tag{28}$$

where L_w is the hydrodynamic inductance of the weak link, and Eq. (18) remains unchanged. Quantization of circulation around an irreducible loop passing through the two passages yields

$$L_m I_m - L_w I_w = n(h/m_4) , \tag{29}$$

where n is an integer characterizing the circulation state. Equation (28) is consistent with n remaining constant in Eq. (29) and may be rewritten in the form

$$\frac{P_2-P_1}{\rho} = -L_r\frac{dI}{dt} , \tag{30}$$

where $L_r = L_w L_m/(L_w+L_m)$. Thus we recover the original set of equations that we had for the main passage alone, but with L_m replaced by L_r.

Note that the currents in Eq. (29) may be regarded as the sums of direct and alternating currents, so that Eq. (29) becomes the two equations

$$L_m I_m(\text{dc}) - L_w I_w(\text{dc}) = n(h/m_4) , \tag{31}$$

$$L_m I_m(\text{ac}) - L_w I_w(\text{ac}) = 0 . \tag{32}$$

In our experiments L_w exceeded L_m by a factor lying between 100 and 10000, so that flow through the main passage dominated the resonance behavior of the cell, and flow through the weak link constituted a relatively minor perturbation of that behavior.

Consider now the effects of the nonlinear dissipation associated with supercritical flow of the superfluid. We assume that such dissipation is associated with the creation and motion of quantum vortices in the liquid. Such dissipation can occur at both the weak link and main passage and will involve complicated hydrodynamics. For the purposes of our model we assume that such dissipation takes place only at the weak link in the manner described in Sec. I A and involves a change of circulation quantum number n by ± 1 as a single vortex moves across or away from the orifice in a time short compared to the period of oscillation. Further, we assume that such dissipation occurs when $|I_w|$ reaches a well-defined critical value I_{wc} which is the same for both directions of flow. Thus we assume that the motion of the fluid is governed at most times by the equations described above with constant n, but that discontinuities in behavior occur, with changes in n, whenever I_w reaches $\pm I_{wc}$.

In detail, we assume that each time I_w reaches $+I_{wc}$, I_w drops to a value such that n changes by $+1$ with no change in I_m. Because this effectively discontinuous change in current flow involves no discontinuity in P_2-P_1, dI/dt will be the same after the jump as before. The new values for n and I and the unchanged value for dI/dt serve as initial conditions for further oscillation governed by the linear equations of motion until once again $|I_w|$ reaches its critical value. Similar remarks apply when I_w reaches $-I_{wc}$, at which point n is assumed to change by -1.

If the foregoing assumptions are satisfied, a plot of the steady-state response amplitude x_0 versus drive amplitude Ω_{2d0} at resonance will show a staircase pattern as shown in Fig. 3, in close analogy with the corresponding characteristic of an rf-biased SQUID.[33,34] This response may be understood as follows.

Suppose that there is a small amount of linear damping in the system, whether due to dissipation in the fluid itself or in the cell walls, which limits the response of the system on resonance and results in high but finite Q values. At low drive amplitudes, I_w will then remain subcritical in steady state, but a plot of x_0 versus Ω_{2d0} will rise steeply from zero in reflection of the high Q value.

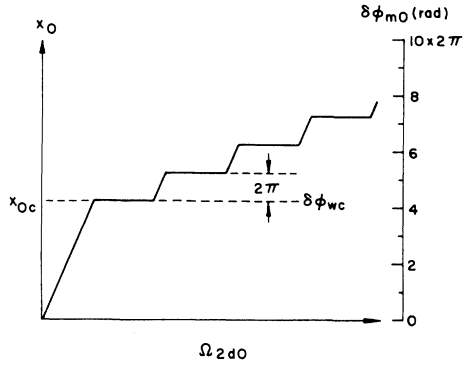

FIG. 3. Hypothetical plot of the anticipated staircase response of lower-diaphragm displacement amplitude x_0 to volume drive amplitude Ω_{2d0} for a case in which $\delta\phi_{wc}=4.25\times 2\pi$ rad.

When Ω_{2d0} attains the level at which $|I_w|$, at its maximum during oscillation, just reaches I_{wc}, a dissipative event will occur. Assume, for example, that I_w is positive at this point and that n was initially zero. Then n becomes $+1$ and I_w is decreased below critical with a loss of energy of oscillation equal to $L_w(I_{wc}^2-I_{wf}^2)/2$, where I_{wf} is the value of I_w immediately after the event. Since $I_{wf}=I_{wc}-(h/m_4)/L_w$, the energy loss equals $(h/m_4)\bar{I}_w$, where $\bar{I}_w\equiv(I_{wc}+I_{wf})/2$.

Because of this energy loss, the amplitude of ensuing oscillation is reduced. However, because this reduction is small under our conditions it is likely that one-half cycle later the critical current will be exceeded in the negative direction because of the bias applied to I_w relative to I_m by the nonzero circulation. When this happens, n will be reset to zero, with further loss of energy of oscillation and reduction of the amplitude of oscillation. This amplitude is regained only on a time scale governed by Q/ω, so that a number of cycles may elapse before further dissipative events can occur.

As Ω_{2d0} is further increased, the recovery of the amplitude of oscillation after such a pair of dissipative events will quicken, but x_0, which will have small sawtooth variations in it, will not on the average increase. Thus, a plateau in the plot of x_0 versus Ω_{2d0} will appear. This plateau will extend to a value of Ω_{2d0} such that the drive can supply sufficient energy in each cycle of oscillation for there to occur four dissipative events during the cycle, with the value of n going through the sequence $0\rightarrow 1\rightarrow 0\rightarrow -1\rightarrow 0$.

For further increases in Ω_{2d0}, x_0 will rise above the plateau until the first transitions to the $n=\pm 2$ states can occur. At this point a second plateau will begin. This plateau will last until Ω_{2d0} is sufficiently large to induce eight transitions per cycle, driving the value of n through the sequence $0\rightarrow 1\rightarrow 2\rightarrow 1\rightarrow 0\rightarrow -1\rightarrow -2\rightarrow -1\rightarrow 0$. After this, a new rise in x_0 will begin, and so forth, as illustrated in Fig. 3. It is the appearance of such a staircase pattern that we seek as a first manifestation of a Josephson effect in our system.

It is useful to relate x_0 to $\delta\phi_{m0}$, the amplitude of the oscillations of the order-parameter phase-difference $\delta\phi$ evaluated along a path passing through the main passage. We assume that flow through this passage remains subcritical and that no vortices cross such a path. From Eq. (11) we obtain

$$\delta\phi_{m0}=-\frac{1}{i\omega\hbar}(\mu_{20}-\mu_{10}) , \tag{33}$$

which when combined with Eq. (20) gives us

$$\delta\phi_{m0}=-\frac{1}{i\omega\hbar}\frac{m_4}{\rho}\frac{k}{A}\frac{\Omega_1+\Omega_2}{\Omega_2}\frac{\omega^2}{\omega_H^2}\frac{(1+\alpha_1)\omega_T^2-\omega^2}{\omega_T^2}x_0 . \tag{34}$$

Thus at any given ω, in particular at resonance, $\delta\phi_{m0}$ is simply proportional to x_0. Any small amount of damping present in the system should not alter Eq. (34) significantly at either ω_+ or ω_-, since typically neither ω_+^2 nor ω_-^2 will be particularly close to $(1+\alpha_1)\omega_T^2$.

Since up to the first plateau the flow through the weak link remains subcritical, $\delta\phi_{w0}=\delta\phi_{m0}$, and thus $\delta\phi_{m0}$ at the first plateau equals $\delta\phi_{wc}$, the phase-difference $\delta\phi$ through the weak link at the critical rate of flow through the weak link. Furthermore, the change in $\delta\phi_{m0}$ between successive plateaus should equal 2π. In order to see this, note that at the onset of the pth plateau, I_w will just be able to reach $+I_{wc}$ with the system in the $(n=p-1)$th state of circulation when I_m reaches its maximum value I_{m0}. As a result, we have at this point

$$\delta\phi_{m0}-\delta\phi_{w0}=\delta\phi_{m0}-\delta\phi_{wc}=2\pi(p-1) \tag{35}$$

and thus

$$\delta\phi_{m0}(p\text{th plateau})=\delta\phi_{m0}(1\text{st plateau})+2\pi(p-1) . \tag{36}$$

The positions of step features along the Ω_{2d0} axis are harder to predict since they depend sensitively on the behavior of the resonator. The length of each plateau along the Ω_{2d0} axis should correspond to an increase in energy dissipated per cycle equal to $4(h/m_4)\bar{I}_w$. However, the accompanying change in work done by the drive diaphragm is not directly related to Ω_{2d0} because it also involves the amplitude and phase of P_2, which will depend sensitively on the dissipation.

Figure 4 represents the steady-state situation that we envision for a value of Ω_{2d0} infinitesimally below that at which the third plateau commences. Because the flow through the main passage will dominate the flow through the weak link, I_m will vary very nearly sinusoidally in time, as will P_2-P_1 and $\delta\phi_m$. The quantities I_w and $\delta\phi_w$ as governed by Eqs. (29) and (5) will then follow I_m and $\delta\phi_m$ with offsets which change whenever a dissipative transition changes the circulation state.

Our model assumes that each time a dissipative transition occurs, the vortex configuration involved moves away from the weak link or is annihilated sufficiently rapidly so that the state of the weak link is effectively reset by the time that I_w next reaches $\pm I_{wc}$. In the situation shown in Fig. 4, it is seen that the reset must occur in less than, say,

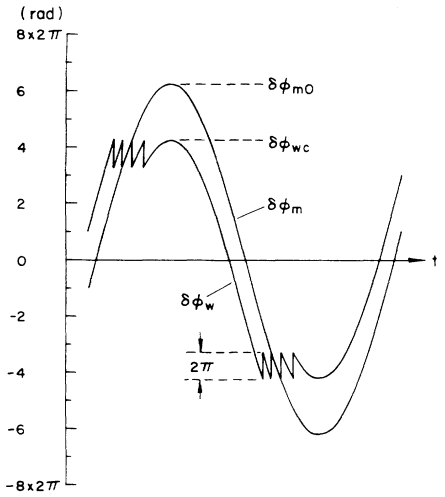

FIG. 4. Plots of the steady-state waveforms of $\delta\phi_m$ and $\delta\phi_w$ expected for the case of Fig. 3 for amplitudes infinitesimally below those at which the third plateau commences.

$\frac{1}{50}$ of a cycle, which would be 20 μs for a frequency of 1 kHz. For critical superfluid velocities of the order of 1 m/s and distances to be covered of the order of 1 μm, the reset time might be expected to be of the order of 1 μs, will within the time limit estimated above.

An extension of the Josephson behavior described above concerns the alteration in the staircase pattern which would be induced by a superimposed steady mass flow through the cell. The effect of such a bias current is closely analogous to the effect of an applied steady magnetic flux through the loop of an rf-biased SQUID.

Let us consider a steady mass current I_b that is introduced from outside into the lower chamber and withdrawn from the upper chamber. The system of equations considered above must be modified by the addition of I_b to the right-hand sides of Eqs. (15) and (16). The addition of such terms has no influence on the oscillatory parts of the solutions in the linear region of behavior. However, the steady part of I_w, as determined by the equations $I_w(\mathrm{dc})+I_m(\mathrm{dc})=I_b$ and $L_mI_m(\mathrm{dc})-L_wI_w(\mathrm{dc})=n(h/m_4)$, is given by the relationship

$$I_w(\mathrm{dc})=\frac{L_m}{L_w+L_m}I_b-\frac{1}{L_w+L_m}n\frac{h}{m_4}\ . \tag{37}$$

Thus the set of values of $I_w(\mathrm{dc})$ for various circulation states is biased by the term involving I_b.

This bias is equivalent to a shift of the critical values of I_w from $\pm I_{wc}$ to $\pm I_{wc}-I_bL_m/(L_w+L_m)$ and will have the effect of splitting each plateau into two subplateaus. This splitting will be periodic in I_b with period $(h/m_4)/L_m$, and a plot of the value of x_0 of any one of the subplateaus versus I_b will yield a symmetrical sawtooth pattern analogous to the sawtooth variation of subplateau response versus applied magnetic flux seen in the rf-biased SQUID.[33] The observation of such an effect in addition to the staircase pattern would give supporting evidence for the existence of a Josephson effect.

III. PROCEDURES AND RESULTS

A. Determination of apparatus parameters

In order to define our observations properly, it was first of all necessary to calibrate our cell thermometers with respect to cell temperature and our lower-diaphragm transducer with respect to static pressure in the cell. Second, we needed to determine the parameters required to calculate the phase difference amplitude $\delta\phi_{m0}$ from measurements of the response voltage amplitude output V_{r0} from our fm detector.

Equation (34) gives $\delta\phi_{m0}$ in terms of the deflection amplitude x_0. The amplitude x_0 is in turn related to the amplitude f_0 of frequency excursions of the rf oscillator by the relation

$$x_0=Bf_0 \tag{38}$$

for the small amplitudes involved, where B is a frequency-dependent constant. Finally, f_0 is proportional to V_{r0} with a constant of proportionality characteristic of the fm detector, 10^5 Hz/V in our measurements. The various parameters involved in relating $\delta\phi_{m0}$ to f_0 may in principle be determined as follows. The quantity $(k/A)B$ can be obtained from static measurements of f versus cell pressure. The chamber volumes may be calculated from the cell dimensions. The angular frequency ω_T may be measured directly by exciting the cell when empty. The quantities α_1 and ω_H can then be calculated from measurements of ω_+ and ω_- with the cell filled, using Eqs. (23) and (24) and the relationship $\alpha_1/\alpha_t=(\Omega_1+\Omega_2)/\Omega_1$.

Knowledge of these parameters also permits us to calculate the volume drive amplitude Ω_{2d0} from measurements of V_{r0}, by making use of Eq. (19). These measurements could be made both on and off resonance. However, when used to interpret measurements on resonance, Eq. (19) needs to be modified to include the effects of damping on the shape of the resonance peak. The volume drive amplitude is related to the voltage drive amplitude V_{d0} applied to the piezoelectric transducer by the equation

$$\Omega_{2d0}=CV_{d0}\ , \tag{39}$$

where C, the driver coefficient, is a constant which might have some pressure dependence. This coefficient can thus be evaluated from time to time as might be needed for a check on the consistency of the performance of our apparatus.

Table I provides a catalog of the 18 principal runs at low temperature that have been made during this work. At the beginning of a run, while the cell was still empty, the frequency f of the deflection-sensing oscillator was recorded over a range of temperatures to provide zero-pressure values. As a representative example, the empty cell frequency in run 18 increased by 1.4 kHz at 8.8 MHz as the cell temperature rose from 0.6 K to T_λ. In addition, a measurement of the lower diaphragm resonant fre-

TABLE I. Catalog of runs at low temperature. In runs 8, 9, and 16 the chambers of the cell were filled with Metricel filter membrane,[a] otherwise they were open. In run 9, a ^{3}He-^{4}He mixture with ^{3}He mole fraction $x=0.01$ was used in place of pure ^{4}He. $\nu_\pm=\omega_\pm/2\pi$.

Run no.	Diameters of the weak link[b] (nm)	Diameter of the main passage[c] (mm)	Covering or filling of main passage	ν_-[d] (Hz)	ν_+[d] (Hz)	$\left[\frac{\delta\phi_{wc}(\text{rad})}{2\pi}\right]_-$[e]	$\left[\frac{\delta\phi_{wc}(\text{rad})}{2\pi}\right]_+$[e]
1	No weak link	0.8	Nuclepore[f]	(642)			
2	300×450	0.8	Nuclepore	(553)		9	
3	290×470	0.8	Nuclepore[g]	(528)		33	
4	150×170	0.8	Powder[h]	(877)		9	
5	90×100	0.8	Powder	834.2		16	
6	150×170[i]	0.8	Powder	(858)		11	
7	No weak link	0.8	Powder	836.3			
8	170×200	0.8	Powder	843.4		33	
9	170×200	0.8	Powder	(829)			
10	240×240	0.8	Open	965.0		32	
11	250×350	0.8	Open	961.9		16	
12	155×185[j]	0.516	Open	779.7		31	
13	155×185	3.2	Open	1177.0		32	
14	155×185	0.287	Open	601.6		31	
15	155×185	0.029	Open	420.0		30	
16	155×185	3.2	Metricel[a]	1152.6		15	
17	155×185	3.2	Open	1179.1	2853.4	17	14
18	155×185	0.287	Open	646.5	2007.8	16	15

[a]1.2-μm pore size (Ref. 30).
[b]Major and minor diameters. The weak-link foil thickness was 100 nm in all cases but run 11, in which it was 200 nm.
[c]The length of the main passage was 0.5 mm in all cases but run 15, in which the passage was a hole in a 5-μm-thick foil.
[d]At $T=0.95$ K, $P\cong 25$ kPa. The values in parentheses were determined at other values of T and P but are representative of the values under these conditions.
[e]At $T=0.95$ K, $P\cong 25$ kPa. See footnote under Ref. 18. For a study of the temperature dependence of $\delta\phi_{wc}$ in runs 12–15, 17, and 18, see Ref. 37.
[f]80-nm pore diameter (Ref. 28).
[g]30-nm pore diameter (Ref. 28).
[h]50-nm particle size (Ref. 27).
[i]The weak link orifice in run 6 was the same one used in run 4 but modified by the addition of surface irregularities and several projections. See Fig. 8 of Ref. 26.
[j]The weak link orifice in runs 12–18 is the same as that in runs 8 and 9 but somewhat reduced in size. See Fig. 5 of Ref. 26.

quency $\nu_T=\omega_T/2\pi$ was made. This resonance could be excited by the driver at relatively high drive levels even though no fluid was present, presumably by shaking the cell body. For example, in runs 16, 17, and 18 ν_T was observed to equal 1120 Hz with very little temperature dependence, the resonance having a Q of 200 000 at 0.65 K.

Next, the cell was filled with liquid ^{4}He, and the lower diaphragm transducer was calibrated with respect to pressure, usually at 0.65 K. This calibration was carried out from ~ 5 to ~ 50 kPa by measuring the deflection-sensing oscillator frequency f as a function of external pressure applied to one or both fill capillaries. The capillaries contained vapor down to some point above the inner ^{4}He pot and liquid from there down to the cell. Consequently, in the presence of large temperature gradients, it might be expected that the cell pressure would differ from the external pressure by a small hydrostatic head and possibly also by a large thermomechanical pressure drop in the portions of the capillaries filled by superfluid. Nevertheless, except under unusual circumstances when the cell had been filled very rapidly, the curve of external pressure versus frequency when extrapolated to the previously mentioned empty-cell frequency almost always yielded a positive value within 1 kPa of zero. We assumed that this offset represented a pressure-independent pressure drop in the capillaries that should simply be subtracted from the external readings to yield the true pressure in the cell. This interpretation was confirmed by one calibration carried out above the lambda point which yielded results almost identical to the low-temperature calibration except for a small offset of opposite sign which could be accounted for by the hydrostatic head alone. Representative values of the frequency were 8.8 MHz at 0 kPa and 6.6

MHz at 50 kPa.

The existence of a calibrated pressure transducer in the cell allowed the germanium cell thermometers to be calibrated *in situ* on the ^{3}He and ^{4}He vapor pressure scales. Calibrations on the T62 ^{3}He scale were carried out during three separate runs over somewhat different ranges of temperature extending from 0.36 to 2.23 K. The agreement in the regions of overlap was excellent. Before the cell was filled with ^{4}He, and thus before the pressure calibration was in fact carried out, enough pure ^{3}He was condensed into the cell to provide coexisting liquid and vapor phases over the range of temperature being studied. In the first of these runs a similar calibration with ^{4}He on the T58 scale was performed. Above 1.24 K the agreement between the ^{3}He and ^{4}He calibrations was also excellent, although the respective vapor pressures were very different. In other runs, the consistent agreement between thermometers lent support to the supposition that neither thermometer had changed calibration between runs.

Once the cell was filled with liquid ^{4}He, the two principal filled-cell resonances at $\nu_\pm = \omega_\pm / 2\pi$ could be located by sweeping the drive frequency from 100 to 4000 Hz and following the response. For much of this work, however, we were unaware of the importance of the lower-diaphragm resonance. As a result, in many runs we did not search for the resonance at ν_+ and we studied only the resonance at ν_-. In these runs, ν_- was measured as a function of temperature at constant pressure over as wide a range of temperature as possible.

In the last two runs we studied both cell resonances from 0.4 K to the vicinity of T_λ. In run 17 we found that the procedure described earlier in this section failed to yield a solution for α_1 and α_t. In the face of this discrepancy we proceeded as if the small volume Ω_1 were unknown. By use of ν_+ and ν_- measured at the same temperature and pressure in both runs 17 and 18, we determined sets of separate values for α_1 and α_t, which were than used to interpret the results of all of our runs. At $T=0.95$ K and $P=25$ kPa, α_1 and α_t equaled 1.85 and 0.52, respectively. The ratio α_1/α_t for these values is 3.6, whereas the ratio $(\Omega_1+\Omega_2)/\Omega_1$ for the volumes computed from cell dimensions is 5.2. The source of this discrepancy is not known. Other indications that our model fails to account accurately for the behavior of the cell were that the temperature dependences of α_1 and α_t as determined here, while similar to each other, were somewhat weaker than that of κ^{-1}. In addition, the temperature dependence of ω_H^2 calculated from the measurements and parameter determinations described above for the last two runs was in one case weaker and in the other stronger than that of $(\rho\kappa)^{-1}$. Other resonances which coupled to the principal resonances were observed in the system, but these subsidiary resonances were all much weaker than the main resonances.

The driver coefficient $C=\Omega_{2d0}/V_{d0}$ was determined using measurements of V_{r0} in relation to V_{d0} both on and off resonance. When evaluated at ν_-, C was found consistently to equal $(5.37\pm0.14)\times10^{-14}$ m^3/V at $T=0.95$ K and $P=25$ kPa. However, when evaluated at ν_+ in the last two runs, C equaled $(3.84\pm0.08)\times10^{-14}$ m^3/V, another indication of inadequacy in the model.

B. Search for a Josephson effect

In order to search for a Josephson effect, the rms response voltage $\tilde{V}_r = V_{r0}/\sqrt{2}$ was observed as slow sweeps of the rms drive voltage $\tilde{V}_d = V_{d0}/\sqrt{2}$ were carried out on resonance at ν_- and also, in the two last runs, at ν_+. A representative plot from run 18 of the results of such a sweep is shown in Fig. 5. Here we see a rapid rise of $\tilde{V}_r$ versus $\tilde{V}_d$ at low levels of $\tilde{V}_d$, corresponding to linear oscillatory behavior with $Q \cong 30\,000$. We interpret the pronounced break in slope at $\tilde{V}_r = 0.43$ mV to mark the first appearance of supercritical flow in the weak link. The subsequent rise, however, shows no sign of the Josephson steps being sought. From the ordinate of the break in slope we calculate that $\delta\phi_{wc} = 17.8\times2\pi$ rad. The pair of short horizontal lines near the curve shows the expected step height for single-quantum transitions, corresponding to a change in $\delta\phi_{m0}$ between plateaus of 2π rad.

These sweeps have been made with both increasing and decreasing amplitude at various rates, with sweeps lasting from several minutes to several hours. The results of a given sweep were in most cases quite reproducible. Although many of the sweeps were carried out at 0.65 K and 25 kPa, many have been made at other pressures, from 13 to 40 kPa, and temperatures, from 0.4 K to T_λ. Our ability to see any step structure that might have been present, however, was dependent on the existence of a sufficiently large change in slope of the response curve at the critical value of $\tilde{V}_r$. Because this change in slope decreased with increasing temperature as a result of the decreasing Q of the resonance, the effective upper tempera-

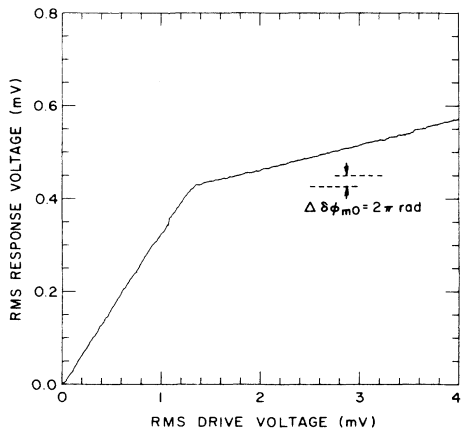

FIG. 5. Representative plot of the rms response voltage $\tilde{V}_r$ versus the rms drive voltage $\tilde{V}_d$ as the drive voltage was slowly increased at the upper resonant frequency. Run 18, $T=0.65$ K, $\nu_+ = 2009.3$ Hz. Note the sharp break in the slope of the curve at $\tilde{V}_r = 0.43$ mV marking the onset of supercritical flow through the weak-link orifice, but no sign of Josephson steps. The pair of dashed horizontal lines shows the step height $\Delta\delta\phi_{m0} = 2\pi$ rad anticipated for single-quantum transitions. $\delta\phi_{wc} = 17.8\times2\pi$ rad.

ture limit of our search for a Josephson effect was ~ 1.1 K.

As shown in Table I, we have made a total of 16 runs with 7 different weak-link orifices and with various main passage configurations. Listed in that table are the values of $\delta\phi_{wc}(\text{rad})/2\pi$ that we obtained, referred to a standard temperature. In only one run, run 2, did we see structure at all suggestive of Josephson step structure. That structure, which was highly reproducible during the run, is shown in Fig. 6. In this case we calculate that $\delta\phi_{wc} = 10.6 \times 2\pi$ rad. Here too, the expected step height for single-quantum transitions is shown by a pair of horizontal lines.

Josephson steps in $\tilde{V}_r$, if present, should also be observable as the drive frequency ν is swept through resonance at constant $\tilde{V}_d$. A set of such sweeps is shown in Fig. 7 for various values of $\tilde{V}_d$, under the same conditions as the drive amplitude sweep shown in Fig. 5. The transition to supercritical flow is clearly seen at a level of $\tilde{V}_r = 0.43$ mV in agreement with Fig. 5. Also in agreement with Fig. 5, no sign of step structure is visible in these curves at values of $\tilde{V}_r$ above the transition. Note that the supercritical parts of the resonance curves in Fig. 7 are asymmetrical, with peaks displaced toward lower frequencies. This direction of displacement is in accord with the simple notion that as flow in the weak link orifice becomes supercritical, the inductance L_w of the weak link effectively increases, causing the parallel combination $L_r = L_w L_m/(L_w + L_m)$ to increase and ω_H to decrease.

For the one orifice which showed a suggestion of step structure in the $\tilde{V}_r$ versus $\tilde{V}_d$ characteristic, curves of $\tilde{V}_r$ versus frequency at drive amplitudes yielding the first plateau were particularly flat on top, and the subsequent rise in $\tilde{V}_r$ above the plateau at higher levels of $\tilde{V}_d$ appeared as a pronounced new peak which was displaced toward lower frequencies from the subcritical location of the original resonance peak.

At much higher drive amplitudes we saw additional nonlinearity which we attribute to supercritical flow taking place in the main passage. This nonlinearity took the form of further reductions in the slopes of curves of $\tilde{V}_r$ versus $\tilde{V}_d$ at resonance as $\tilde{V}_d$ was increased. These reductions were sometimes accompanied by abrupt and nonreproducible jumps in $\tilde{V}_r$, as if over some interval of drive amplitude the system could exist in either of two states, one with, the other without the occurrence of additional dissipation in the main passage. In run 15, in which the main passage consisted of an orifice in a 5-μm-thick copper foil, we observed that when supercritical flow took place in that passage, the oscillation waveform was actually undergoing a series of sudden collapses, each followed by a period of slower regrowth. This behavior, which has been seen in other work with superfluid ^{4}He Helmholtz resonators,[35] was presumably due to the energy stored in the resonant oscillation being released in a burst of vortex creation and motion initiated by supercritical flow through the main passage and then being restored more gradually by the drive at subcritical rates of flow.

The additional nonlinearity that we attribute to supercritical flow in the main passage was also seen as a further flattening of curves of $\tilde{V}_r$ versus ν as ν was swept through resonance. Unlike the flattening at lower drive amplitudes associated with supercritical flow in the weak link, the flattening here preserved the symmetry of the curve without any further frequency shift of the peak.

In order to verify that the first nonlinear effects that we observed at low drive amplitudes were indeed associated with supercritical flow in the weak-link orifice, we made

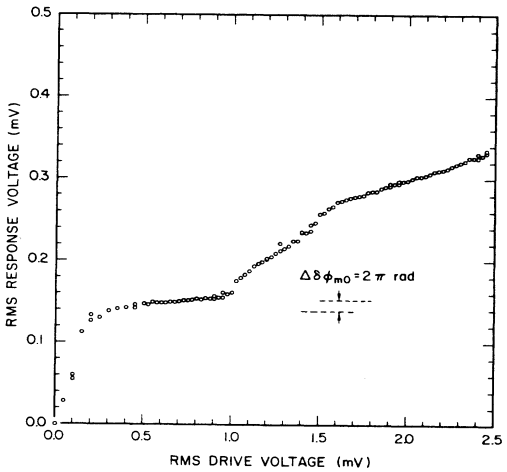

FIG. 6. Root-mean-square response voltage $\tilde{V}_r$ versus rms drive voltage $\tilde{V}_d$ at the lower resonant frequency. Run 2, $T = 0.65$ K, $\nu_- = 553$ Hz. Note the suggestion of multiple steps. The pair of dashed horizontal lines shows the step height $\Delta\delta\phi_{m0} = 2\pi$ rad anticipated for single-quantum transitions. $\delta\phi_{wc} = 10.6 \times 2\pi$ rad.

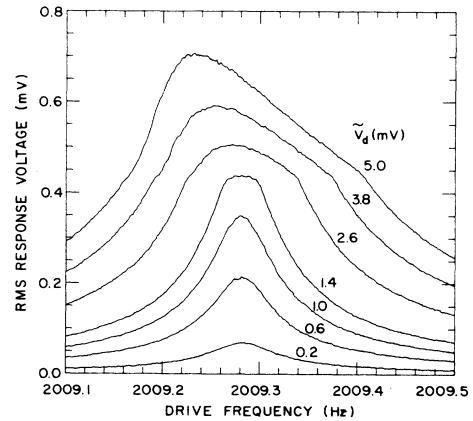

FIG. 7. Representative plots of the rms response voltage $\tilde{V}_r$ versus the drive frequency ν as the frequency was slowly increased at several different values of the rms drive voltage $\tilde{V}_d$. The conditions were the same as for Fig. 5. Note the flattening and the frequency shift of the peaks for $\tilde{V}_r$ in excess of the critical value 0.43 mV.

runs on two separate occasions with no weak link present. In these runs, runs 1 and 7, no breaks were seen at low drive amplitudes in curves of $\tilde{V}_r$ versus either $\tilde{V}_d$ or ν, and linearity of response extended up to the $\tilde{V}_r$ levels at which the supercritical effects that we attribute to the main passage typically appeared.

Careful attention was paid to the noise present in the system. Of particular concern was any noise which represented random excitation of the principal resonances; such noise would have tended to average out any step structure. In assessing such noise care was taken to avoid using a lock-in output time constant longer than the decay time constants of the resonances.

Low-frequency noise in the lock-in output was quite variable from day to day and run to run. We convinced ourselves, by the use of varying degrees of vibration isolation of the entire cryostat and by the use of vibration generators and detectors on the outside of the cryostat, that sources of vibration external to the cell, including boiling in the liquid-helium and liquid-nitrogen baths, were not the main causes of this noise. Furthermore, we eventually found that the noise level seemed to be correlated with the speed with which the cell had been filled. Our usual practice was to fill the cell while it was held at a temperature well below T_λ. Exceptionally quiet behavior was observed during our last run, after the cell was filled at such a temperature quite slowly, over a period of 5 h, a packed-powder superleak having been placed at the cell entrance through which filling took place. On the other hand, the cell had been found in a particularly noisy state which persisted for several days after a more rapid filling than usual had occurred during the previous run. These observations suggest that the noise seen here was due to remnant vorticity of the superfluid either in the cell or fill capillaries. Other work has shown that such vorticity may persist for long periods of time.[36]

Once the cell was filled, warming the cell above T_λ and recooling it sometimes influenced the noise and sometimes did not. Unfortunately, during the runs in which this procedure was carried out in the presence of a relatively large amount of noise, the liquid in the cell fill capillaries was allowed to remain below T_λ and may have served as a reservoir of quantum vorticity. Curiously enough, the amount of noise present did not seem to depend on how strongly the cell resonances had been excited, even though supercritical levels of oscillation should have produced more vorticity in the superfluid. In any event, as illustrated in Figs. 5 and 7, we were able on at least some occasions to carry out our search with noise levels in $\tilde{V}_r$ significantly less than the separation expected between adjacent Josephson plateaus.

In run 9 we filled the cell with a ^{3}He-^{4}He mixture having a ^{3}He mole fraction of 0.01. Although the Q of the lower resonance studied was significantly reduced by the presence of the ^{3}He, the usual sharp onset of supercritical flow in the weak link was seen, but no sign of step structure was visible.

IV. CONCLUSIONS AND DISCUSSION

We have described a search for an ac Josephson effect in superfluid ^{4}He which was carried out by a different method than used in previous searches, under conditions which we believe to have been more favorable than in those searches. Nevertheless, except for the suggestive results of an early run which have failed to appear in subsequent runs with different weak links, the present experiments have not succeeded in detecting an ac Josephson effect in superfluid ^{4}He.

Because the effect being sought is based upon the rather well-established principles of two-fluid dynamics and quantization of superfluid circulation, it is important to try to understand why the effect might not have been observed. Let us assume that Eq. (11), the ac Josephson equation for superfluid ^{4}He, relating fluid acceleration and order-parameter phase-slip by vortex motion to differences in the chemical potential, is valid, and that the failure of the Josephson effect to be observed is really the failure of the phase slip to be properly synchronized with the resonant oscillations of the system. There are several possibilities to be considered.

First, the critical phase difference must be sharply defined and highly reproducible relative to the step height 2π. Otherwise, the step structure will be averaged out. Although, as illustrated in Fig. 5, our critical level, which reflects the average of many individual transitions, can be rather well-defined, it is not clear that the individual transitions themselves are reproducible enough.

Second, the amount of phase slip or the change in circulation state which occurs at each transition must be highly reproducible, or again, the step structure will be averaged out. The change in circulation state at each transition need not be ± 1 as assumed in Sec. II B; for regular step structure to occur it could just as well be $\pm m$, where m is any positive integer, as long as m is the same for all transitions. As is shown in Table I, our goal of finding weak-link orifices with critical phase differences close to 2π was not achieved. The values of $\delta\phi_{wc}/2\pi \gg 1$ which were obtained offered wide ranges of possible values of Δn leading to lower-energy states of flow once $\delta\phi_{wc}$ was reached. The irregular collapse of the resonant amplitude that has been seen in other work on superfluid Helmholtz resonators with relatively large openings, and which has been seen in this work for supercritical flow through a main passage in the form of an orifice in a thin film, is an example of a highly nonreproducible phase slip of many factors of 2π that can occur when a critical phase difference has been reached.

We found in general that $\delta\phi_{wc}$ decreased with increasing temperature,[37] presumably going to zero at T_λ. Because this result suggests that more favorable conditions for reproducible phase slip might exist near T_λ, it is unfortunate that our technique is limited to temperatures well below T_λ.

The uncertainty concerning the two possibilities above reflects our lack of understanding about what determines the critical flow condition and what happens after it is reached. The critical velocities corresponding to the observed critical phase differences may be estimated from the diameters of the orifices and thicknesses of the foils using the following relationship

$$v_{sc} = \frac{\hbar}{m_4} \frac{\delta\phi_{wc}}{l_{\mathrm{eff},w}} \ . \tag{40}$$

Here v_{sc} is the superfluid velocity averaged over the minimal cross-sectional area of the weak-link orifice at the critical rate of flow, and $l_{\text{eff},w}$ is the effective hydrodynamic length of the orifice introduced in Sec. I A. For a long circular-cylindrical pore of length l and diameter d, l_{eff} is approximately equal to $l+8d/3\pi$, whereas for a circular orifice in an ideally thin wall, l_{eff} equals $\pi d/4$. Using the former, we find critical velocities ranging from 2 to 13 m/s for the various orifices at 0.95 K and ~ 25 kPa. These velocities are roughly one order of magnitude less than the Landau critical velocity of ~ 60 m/s.

One should consider the possibility that at the tip of some random projection into the orifice the velocity reaches a critical value locally when the value of average velocity in the orifice is much lower. Such a projection might serve as a nucleation center for vortex creation and growth and thus for phase slip. The question of whether a nucleated vortex could escape from such a projection is an important one. Between runs 4 and 6 projections were intentionally grown into the orifice used in these runs, but very little change in critical phase difference was observed.

A third possibility for the failure of a Josephson effect to be observed concerns the possible motion of free vortices in the chambers. Consider, in the absence of oscillation, the change in the steady value of I_w which will occur as a vortex line is formed, moves, and disappears in such a way as to change by one quantum unit the circulation around an irreducible contour which threads the two openings between chambers. A two-dimensional equivalent of this process is illustrated in Fig. 8. Because $L_w \gg L_m$ and because $I_w = -I_m$ in this case, most of the contribution to the circulation around such a contour in the absence of a vortex will come from the flow through the weak link. In this case we will have $\delta\phi_w \cong -2\pi n$, where n is the circulation quantum number. Hence as the vortex forms, moves, and disappears, $\delta\phi_w$ must change continuously by $\pm 2\pi$. As a result, with the vortex present there will be a bias to the flow through the weak link similar to that discussed earlier for steady flow from chamber to chamber induced from outside. Thus the vortex motion described above would carry the oscillatory response of the cell on one of the plateaus through one cycle of the "sawtooth pattern."

If such vortex motion were to take place in a time comparable to or less than the time required to measure the response, the response would represent some average over the sawtooth pattern at each drive amplitude, and the staircase pattern would tend to be averaged out. The filling of the chambers with porous material in runs 8, 9, and 16 was made in attempt to prevent the motion of free vortices in the chambers. However, no positive results of this filling were seen, and the filling seemed to lower the Q of the resonance.

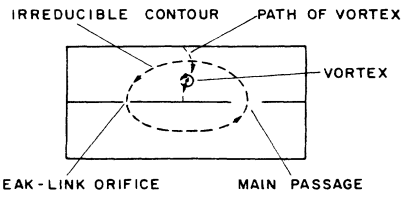

FIG. 8. Schematic diagram of the interior of the cell showing (in two dimensions) a representative vortex path that crosses any irreducible contour threading the two passages between chambers.

In conclusion, although there seem to be no fundamental reasons why an ac Josephson effect should not be observable in superfluid ^{4}He, there are several possible effects which may prevent such an effect from being seen in any given experiment. One of these is irregular phase slip at the weak link; another is an effective loss of long-range phase coherence in the liquid due to the motion of free vortices. The recently reported success of the closely related experiment by Avenel and Varoquaux gives encouragement that under the right conditions sufficiently regular phase slip at an orifice can indeed be achieved.[19] Their work suggests the possible importance of using repetition rates of a few hertz and temperatures of the order of 10 mK, although they were able to observe regular phase slip up to 0.8 K. Their success with an orifice in the form of a narrow slot raises the question of whether noncircular shapes are more favorable than circular ones.

ACKNOWLEDGMENTS

We are particularly indebted to F. H. Wirth, who began these experiments. We also wish to thank B. J. Anderson for help in instrumentation and data taking. We are grateful for the support provided for this work by the Graduate School of the University of Minnesota and the National Science Foundation under Grant No. DMR 81-12973.

[1]B. D. Josephson, Phys. Lett. **1**, 251 (1962); Rev. Mod. Phys. **36**, 216 (1964); Adv. Phys. **14**, 419 (1965).
[2]P. L. Richards and P. W. Anderson, Phys. Rev. Lett. **14**, 540 (1965).
[3]P. W. Anderson, in *Quantum Fluids*, edited by D. F. Brewer (North-Holland, Amsterdam, 1966), p. 146; Rev. Mod. Phys. **38**, 298 (1966).
[4]B. M. Khorana and B. S. Chandrasekhar, Phys. Rev. Lett. **18**, 230 (1967).
[5]B. M. Khorana, Phys. Rev. **185**, 299 (1969).
[6]P. L. Richards, Phys. Rev. A **2**, 1532 (1970).
[7]R. W. Guernsey, Jr., in *Proceedings of the Twelfth International Conference on Low Temperature Physics*, edited by E. Kanda (Keigaku, Tokyo, 1971), p. 79.
[8]G. L. Schofield, Jr., Ph.D. dissertation, University of Michigan, 1971, available from University Microfilms International, Ann Arbor, MI 48106.
[9]J. P. Hulin, C. Laroche, A. Libchaber, and B. Perrin, Phys. Rev. A **5**, 1830 (1972).
[10]D. L. Musinski and D. H. Douglass, Phys. Rev. Lett. **29**, 1541 (1972).
[11]D. L. Musinski, J. Low Temp. Phys. **13**, 287 (1973).

[12]P. Leiderer and F. Pobell, Phys. Rev. A **7**, 1130 (1973).
[13]G. Gamota, Phys. Rev. Lett. **33**, 1428 (1974).
[14]P. W. Anderson and P. L. Richards, Phys. Rev. B **11**, 2702 (1975).
[15]A. G. M. Van der Boog, Ph.D. thesis, University of Leiden, Netherlands, 1979.
[16]I. Rudnick, Phys. Rev. A **8**, 1969 (1973).
[17]F. H. Wirth and W. Zimmermann, Jr., Physica **107B**, 579 (1981).
[18]B. J. Anderson, B. P. Beecken, and W. Zimmermann, Jr., in *Proceedings of the Seventeenth International Conference on Low Temperature Physics,* edited by U. Eckern, A. Schmid, W. Weber, and H. Wühl (North-Holland, Amsterdam, 1984), Part I, p. 313. Note that five of the runs listed in Table I of the present article (runs 5, 4, 8, 2, and 3) coincide with the runs listed in Table I of this reference. The values of $\delta\phi_{wc}/2\pi$ given in the present article include the effects of the lower-diaphragm resonance and of temperature, which were not taken into account in this reference.
[19]O. Avenel and E. Varoquaux, Phys. Rev. Lett. **55**, 2704 (1985); O. Avenel, Bull. Am. Phys. Soc. **31**, 795 (1986).
[20]I. M. Khalatnikov, *An Introduction to the Theory of Superfluidity* (Benjamin, New York, 1965).
[21]E. R. Huggins, Phys. Rev. A **1**, 332 (1970). The result given in our Eq. (14) can be shown to equal Huggins's $\kappa\dot{J}_{\phi\text{crossed}}$.
[22]B. S. Deaver, Jr. and J. M. Pierce, Phys. Lett. **38A**, 81 (1972).
[23]P. W. Anderson and A. H. Dayem, Phys. Rev. Lett. **13**, 195 (1964).
[24]R. P. Feynman, in *Progress in Low Temperature Physics,* edited by C. J. Gorter (North-Holland, Amsterdam, 1957), Vol. I, Chap. II.
[25]Stycast 1266, Emerson and Cuming, Canton, MA 02021.
[26]B. P. Beecken and W. Zimmermann, Jr., J. Vac. Sci. Technol. A **3**, 1839 (1985).
[27]Linde B alumina abrasive, Linde Div., Union Carbide Corp., Danbury, CT 06817.
[28]Nuclepore polycarbonate membrane, Nuclepore Corp., Pleasanton, CA 94566.
[29]Berylco 25, Berylco, Reading, PA 19603.
[30]Metricel GA-3, Gelman Instrument Co., Ann Arbor, MI 48106.
[31]PZT-4, Vernitron Piezoelectric Division, Bedford, OH 44146.
[32]J. S. Brooks, B. B. Sabo, P. C. Schubert, and W. Zimmermann, Jr., Phys. Rev. **19**, 4524 (1979).
[33]O. V. Lounasmaa, *Experimental Principles and Methods Below 1 K* (Academic, New York, 1974).
[34]M. Tinkham, *Introduction to Superconductivity* (McGraw-Hill, New York, 1975).
[35]G. B. Hess, Phys. Rev. B **15**, 5204 (1977).
[36]D. D. Awschalom and K. W. Schwarz, Phys. Rev. Lett. **52**, 49 (1984).
[37]B. P. Beecken and W. Zimmermann, Jr., Phys. Rev. B (to be published).